Spectral optical properties of Cu_2ZnSnS_4 thin film between 0.73 and 6.5 eV

Jian Li,[1,2,*] Hui Du,[1] John Yarbrough,[1] Andrew Norman,[1] Kim Jones,[1] Glenn Teeter,[1] Fred Lewis Terry Jr.,[2] and Dean Levi[1]

[1]*National Renewable Energy Laboratory, 1617 Cole Boulevard, Golden, Colorado 80401, USA*
[2]*Department of Electrical Engineering and Computer Science, University of Michigan, 1301 Beal Avenue, Ann Arbor, Michigan 48109, USA*
[*]*Jian2.Li@nrel.gov*

Abstract: A polycrystalline Cu_2ZnSnS_4 thin film was deposited on fused quartz by co-evaporation. The selected thickness was ~100 nm to avoid artifacts in its optical properties caused by thicker as-grown films. The composition and phase of the film were checked with x-ray fluorescence, Raman shift spectroscopy, scanning transmission electron microscopy, and energy dispersive x-ray spectroscopy. An improved spectroscopic ellipsometry methodology with two-side measurement geometries was applied to extract the complex dielectric function $\varepsilon = \varepsilon_1 + i\varepsilon_2$ of the Cu_2ZnSnS_4 thin film between 0.73 and 6.5 eV. Five critical points were observed, at 1.32 (fundamental band gap), 2.92, 3.92, 4.96, and 5.62 eV, respectively. The ε spectra are in reasonable agreement with those from theoretical calculations.

OCIS codes: (120.0120) Instrumentation, measurement, and metrology; (120.2130) Ellipsometry and polarimetry; (160.2100) Electro-optical materials; (310.6860) Thin films, optical properties.

References and links

1. P. Jackson, D. Hariskos, E. Lotter, S. Paetel, R. Wuerz, R. Menner, W. Wischmann, and M. Powalla, "New world record efficiency for Cu(In,Ga)Se_2 thin-film solar cells beyond 20%," Prog. Photovolt. Res. Appl. **19**(7), 894–897 (2011).
2. H. Katagiri, K. Jimbo, W. S. Maw, K. Oishi, M. Yamazaki, H. Araki, and A. Takeuchi, "Development of CZTS-based thin film solar cells," Thin Solid Films **517**(7), 2455–2460 (2009).
3. B. Shin, O. Gunawan, Y. Zhu, N. A. Bojarczuk, S. J. Chey, and S. Guha, "Thin film solar cell with 8.4% power conversion efficiency using an earth abundant Cu_2ZnSnS_4 absorber," Prog. Photovolt. Res. Appl. n/a (2011), doi:10.1002/pip.1174.
4. D. A. R. Barkhouse, O. Gunawan, T. Gokmen, T. K. Todorov, and D. B. Mitzi, "Device characteristics of a 10.1% hydrazine-processed $Cu_2ZnSn(Se,S)_4$ solar cell," Prog. Photovolt. Res. Appl. (2011), doi:10.1002/pip.1160.
5. J. S. Seol, S. Y. Lee, J. C. Lee, H. D. Nam, and K. H. Kim, "Electrical and optical properties of Cu_2ZnSnS_4 thin films prepared by rf magnetron sputtering process," Sol. Energy Mater. Sol. Cells **75**(1–2), 155–162 (2003).
6. Y. Miyamoto, K. Tanaka, M. Oonuki, N. Moritake, and H. Uchiki, "Optical Properties of Cu_2ZnSnS_4 Thin Films Prepared by Sol–Gel and Sulfurization Method," Jpn. J. Appl. Phys. **47**(1), 596–597 (2008).
7. S. Levcenko, G. Gurieva, M. Guc, and A. Nateprov, "Optical constants of Cu_2ZnSnS_4 bulk crystals," Moldavian J. Phys. Sci. **8**(2), 173–177 (2009).
8. R. W. Collins and A. S. Ferlauto, *Optical Physics of Materials* in *Handbook of Ellipsometry*, edited by H. G. Tompkins and E. A. Irene (William Andrew, Norwich, 2005), chap. 2.
9. S. G. Choi, J. Zúñiga-Pérez, V. Muñoz-Sanjosé, A. G. Norman, C. L. Perkins, and D. H. Levi, "Complex dielectric function and refractive index spectra of epitaxial CdO thin film grown on *r*-plane sapphire from 0.74 to 6.45 eV," J. Vac. Sci. Technol. B **28**(6), 1120–1124 (2010).
10. K. Wang, O. Gunawan, T. Todorov, B. Shin, S. J. Chey, N. A. Bojarczuk, D. Mitzi, and S. Guha, "Thermally evaporated Cu_2ZnSnS_4 solar cells," Appl. Phys. Lett. **97**(14), 143508 (2010).
11. G. Teeter, H. Du, J. E. Leisch, M. Young, F. Yan, S. W. Johnston, P. Dippo, D. Kuciauskas, M. J. Romero, P. Newhouse, S. E. Asher, and D. S. Ginley, "Combinatorial study of thin-film Cu_2ZnSnS_4 synthesis via metal precursor sulfurization," in *Proceedings of 35th IEEE Photovoltaic Specialists Conference*, (IEEE, 2010), pp. 650–655.
12. P. A. Fernandes, P. M. P. Salomé, and A. F. da Cunha, "Growth and Raman scattering characterization of Cu_2ZnSnS_4 thin films," Thin Solid Films **517**(7), 2519–2523 (2009).

#160784 - $15.00 USD Received 19 Jan 2012; revised 13 Feb 2012; accepted 17 Feb 2012; published 7 Mar 2012

13. X. Fontané, L. Calvo-Barrio, V. Izquierdo-Roca, E. Saucedo, A. Pérez-Rodriguez, J. R. Morante, D. M. Berg, P. J. Dale, and S. Siebentritt, "In-depth resolved Raman scattering analysis for the identification of secondary phases: characterization of Cu_2ZnSnS_4 layers for solar cell applications," Appl. Phys. Lett. **98**(18), 181905 (2011).
14. K. Wang, B. Shin, K. B. Reuter, T. Todorov, D. B. Mitzi, and S. Guha, "Structural and elemental characterization of high efficiency Cu_2ZnSnS_4 solar cells," Appl. Phys. Lett. **98**(5), 051912 (2011).
15. D. E. Aspnes, "Local-field effects and effective-medium theory: a microscopic perspective," Am. J. Phys. **50**(8), 704–709 (1982).
16. R. M. A. Azzam and N. M. Bashara, *Ellipsometry and Polarized Light*, (North-Holland, 1977).
17. M. I. Alonso, K. Wakita, J. Pascual, M. Garriga, and N. Yamamoto, "Optical functions and electronic structure of $CuInSe_2$, $CuGaSe_2$, $CuInS_2$, and $CuGaS_2$," Phys. Rev. B **63**(7), 075203 (2001).
18. H. Zhao and C. Persson, "Optical properties of $Cu(In,Ga)Se_2$ and $Cu_2ZnSn(S,Se)_4$," Thin Solid Films **519**(21), 7508–7512 (2011).

1. Introduction

Cu_2ZnSnS_4 (CZTS) has gained wide attention in recent years as an absorber material for thin film photovoltaic (PV) applications. Compared to the PV technology based on a similar material - $Cu(In_{1-x}Ga_x)Se_2$ (CIGS), which holds the highest energy conversion efficiency among all thin film PV technologies [1], Cu_2ZnSnS_4 has the advantages of (1) being composed of earth abundant elements, and (2) being less toxic [2]. Thin film solar cells based on a Cu_2ZnSnS_4 absorber layer have reached an efficiency of 8.4% and those based on a $Cu_2ZnSn(SSe)_4$ absorber layer have reached an efficiency of 10.1% [3, 4], demonstrating the promising prospect of the Cu_2ZnSnS_4 technology.

Despite its technical importance, the spectral optical properties of Cu_2ZnSnS_4 have only been studied briefly. Most of past works were focused on the narrow spectral range near the absorption onset to deduce the band gap [5, 6]. Levcenko *et al*. reported the complex dielectric function ε of what was believed to be Cu_2ZnSnS_4 bulk crystals in the spectral range of 0.8 – 4.7 eV [7]. In that pioneering work, however, the pseudo dielectric function $\langle\varepsilon\rangle$ was treated as the intrinsic optical property of Cu_2ZnSnS_4, based on the assumption of a perfect surface without any over-layer. This simplification may account for the artifact of non-zero ε_2 (~0.5) and poorer model fit below the absorption onset, which also puts ε in the higher spectral range under question to certain extent. Such a problem was removed in this work, partially by including a surface over-layer in the data analyses. In addition, the spectral range in this study was expanded to 0.73 – 6.5 eV, such that two more critical points (CP) were observed and quantified [8].

2. Experimental details

The subject of this investigation is a Cu_2ZnSnS_4 thin film, which is more relevant to PV technologies than the Cu_2ZnSnS_4 bulk crystals. A conventional approach of studying PV thin films is to ellipsometrically characterize films more than 1 μm thick after chemo-mechanically polishing the surface [9]. However, for Cu_2ZnSnS_4 solar cells, the optimum Cu_2ZnSnS_4 layer thickness is significantly smaller than 1 μm [3, 10]. Films so thin are subjected to possible damage caused by the polishing process. On the other hand, significant surface over-layers observed to develop on as-grown films thicker than ~200 nm can cause artifacts in the analysis of their optical properties. As a result, the Cu_2ZnSnS_4 film thickness was selected to be ~100 nm. Theoretically, a small thickness may broaden the CP features due to enhanced carrier scattering, but this should not prevent the CP energies, that are closely related to the band structure, from being intrinsic to Cu_2ZnSnS_4 [8].

The Cu_2ZnSnS_4 thin film of this study was deposited using co-evaporation of Cu, Zn, and Sn from three independent effusion cells. Sulfur was supplied with a valved cracking source with cracking zone temperature of 1100 K. The glass substrate was GE 124 fused quartz. Such a substrate provides: (1) a good interface to the deposited film, as the surface roughness measured by spectroscopic ellipsometry (SE) prior to the deposition was negligible; and (2) optical transparency throughout the entire spectral range of this study, enabling ellipsometry measurements from both the film side and through the glass substrate. During the deposition,

#160784 - $15.00 USD Received 19 Jan 2012; revised 13 Feb 2012; accepted 17 Feb 2012; published 7 Mar 2012

the substrate was heated to approximately 450°C. Information on the elemental sources and deposition control process can be found elsewhere [11].

X-ray fluorescence (XRF) measurements of the deposited film indicate that the atomic percentages of the metal elements are Cu: 48.4%, Zn: 26.4%, and Sn: 25.2%. To check the possible existence of secondary phase materials, such as the ternary (Cu_2SnS_3, Cu_3SnS_4…) or the binary (Cu_2S, ZnS, Sn_2S_3…) compounds, a mapping of Raman shift spectra with a spatial step of 1 mm in both the x and y directions was performed in the entire sample area, using a diode laser with a wavelength of 784.2 nm and a power of 100 mW. Figure 1(a) shows a typical Raman spectrum in the area with no sign of secondary phases: all of the peaks near 257, 287, 338, and 370 cm^{-1} can be attributed to Cu_2ZnSnS_4 [12–14]. In addition, the deduced optical property of the Cu_2ZnSnS_4 thin film, to be described in the next section, indicates that the penetration depth of the light with a wavelength of 784.2 nm is ~265 nm, much larger than the film thickness. Therefore, the Raman spectra are representative of the entire film, not only the near surface part.

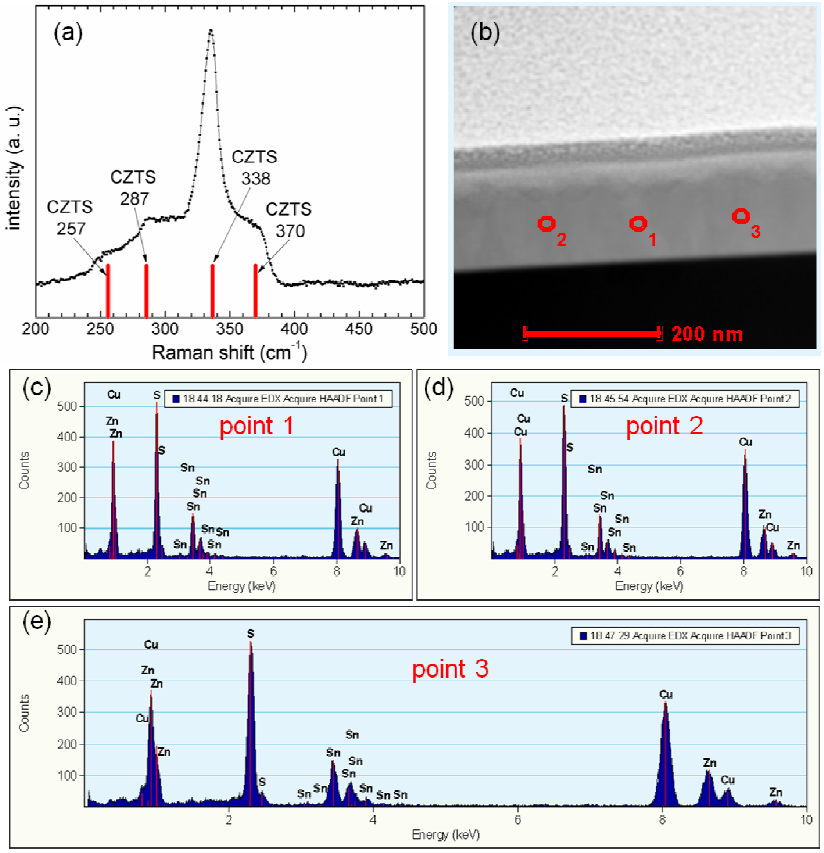

Fig. 1. A typical Raman shift spectrum (a), and a scanning transmission electron microscopy image (b) taken in the phase-pure Cu_2ZnSnS_4 areas of the thin film. Energy dispersive X-ray spectroscopy on the selected points marked in (b) are depicted in panels (c) - (e). Panel (e) was drawn on an expanded x scale to show the details.

To confirm the phase purity as determined above, selected phase-pure Cu_2ZnSnS_4 areas were further characterized using high angle annular dark field (HAADF) scanning transmission electron microscopy (STEM) imaging and energy dispersive X-ray spectroscopy (EDX) analysis performed in an FEI F20 Ultratwin field emitting gun STEM operated at 200 kV. Electron transparent, cross-section STEM samples were prepared using the focused ion beam (FIB) lift out method. The contrast in HAADF images is sensitive to the atomic number

#160784 - $15.00 USD Received 19 Jan 2012; revised 13 Feb 2012; accepted 17 Feb 2012; published 7 Mar 2012

(approximately to the power of 2) and would thus be expected to show strong contrast differences between grains that differ significantly in average atomic number, e.g., as a result of the existence of secondary phases in addition to Cu_2ZnSnS_4. Such differences were not observed in the STEM images as exemplified in Fig. 1(b). EDX analysis was performed on the selected points of Fig. 1(b) with a ~1 nm diameter electron probe, using a Li drifted Si detector unit, after tilting the sample 10 degrees towards the EDX detector to increase the X-ray count rate. Similar EDX spectra, that contain all of Cu, Zn, Sn, and S, were obtained as shown in Fig. 1(c)–1(e). No indication of the existence of secondary phases was observed.

Spectroscopic ellipsometry (SE) was then performed, using a rotating compensator ellipsometer (J.A. Woollam Co. M-2000), on the phase-pure Cu_2ZnSnS_4 areas as determined above. The SE measurement geometries are shown in Fig. 2. Both the film side and through-glass SE were carried out at multiple angles of incidence (AOI) between 40° and 70°. A pair of focusing optics were used in order to: (1) eliminate the unwanted reflections at the glass/air interface from the probing beams reflected at the glass/film interface, and (2) reduce the size of the probing beam to ≤ 1 mm so that only the phase-pure Cu_2ZnSnS_4 areas were measured.

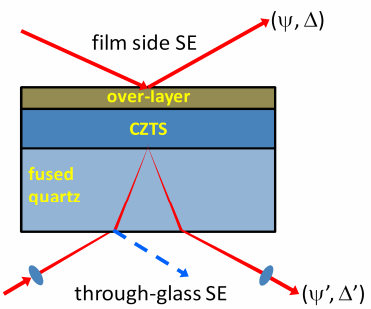

Fig. 2. The measurement geometries for the spectroscopic ellipsometry performed in this study.

In the SE analysis, the deposited film was assumed to have a two layer structure: a Cu_2ZnSnS_4 layer and a surface over-layer. The optical properties of each of these two layers were coupled in the analyses of the SE data from both measurement geometries: film side and through-glass. The thicknesses of these two layers, however, were not coupled to account for possible thickness non-uniformity.

It was observed that, if the surface over-layer was assumed to be a mixture of the underlying Cu_2ZnSnS_4 and variable amount of void to model the surface roughness, whose optical property can be calculated from the effective medium theories [15], unphysical features in the dielectric function of Cu_2ZnSnS_4 would result. This indicates the complexity of the surface over-layers, which may include the surface roughness, the oxides whose optical properties are not known, or a combination of these two non-idealities. In addition, the effective medium theories provide only approximations of the optical property of the surface over-layer, to which SE is highly sensitive.

To address the difficulty commonly seen in similar SE analyses described above, in this study, the spectral optical properties of both the Cu_2ZnSnS_4 layer and the surface over-layer were allowed to vary wavelength-by-wavelength without any assumption in their lineshapes. Compared to traditional SE methodologies, this is a significant relaxation in the assumption of the surface over-layer, which was inapplicable when only one-side SE measurements were performed even at multiple AOIs, due to the strong correlation between two sets of optical properties. Such a correlation was resolved by combining two-side SE geometries and multiple AOIs shown in Fig. 2, as the film side SE is sensitive to the surface over-layer and at the same time the through-glass SE is more sensitive to the Cu_2ZnSnS_4 layer.

#160784 - $15.00 USD Received 19 Jan 2012; revised 13 Feb 2012; accepted 17 Feb 2012; published 7 Mar 2012

3. Results and discussions

Figure 3 shows the measured and the best fit spectra of the ellipsometric angles (ψ, Δ) [16]. The film side and the through-glass SE have significantly different dispersion patterns in (ψ, Δ), and thus provide sufficient information to extract the optical as well as the structural properties of the film. The analysis of Fig. 3 returned the complex dielectric function ε of the Cu_2ZnSnS_4 layer, with all ε_2 approaching or equal to zero below the absorption onset near 1.0 eV as shown in Fig. 4 (solid curves), together with a Cu_2ZnSnS_4 layer thickness of 103.9 ± 0.1 nm and 104.8 ± 0.1 nm, a surface over-layer thickness of 20.5 ± 0.08 nm and 19.7 ± 0.1 nm, for the measured spot in the film side and through-glass SE, respectively. The thickness uncertainties are 90% confidence limits in the fit.

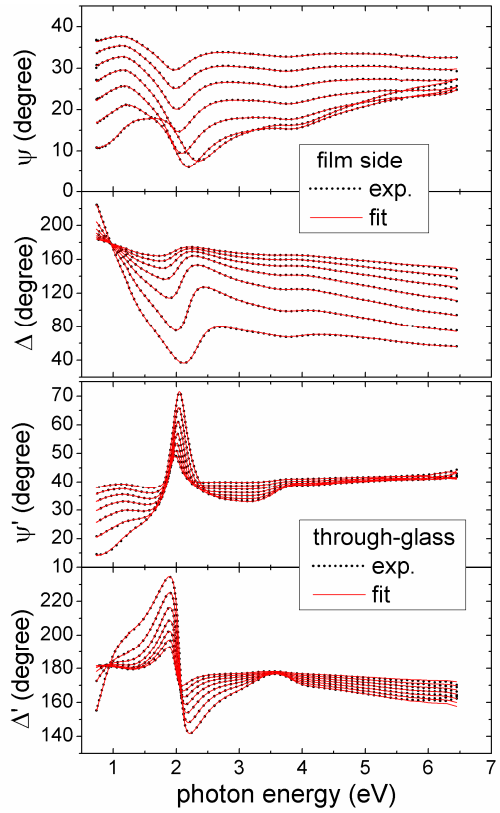

Fig. 3. The film side (upper) and through-glass (lower) SE spectra of the Cu_2ZnSnS_4 thin film.

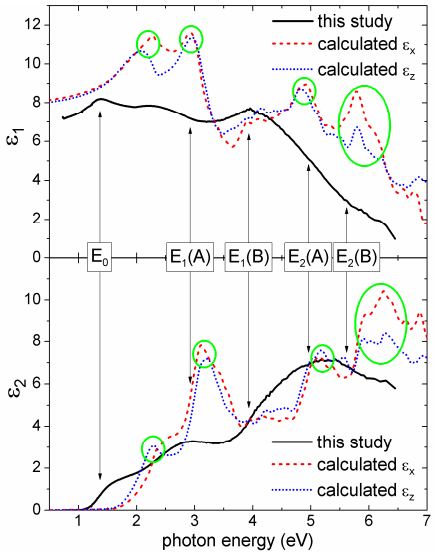

Fig. 4. The real (upper) and imaginary (lower) part of the complex dielectric function ε of the Cu_2ZnSnS_4 thin film of this study (solid curves). The observed critical points are marked with arrows. The experimental ε spectra are compared with the ordinary (ε_x, dashed curves) and extraordinary (ε_z, dotted curves) ε spectra from theoretical calculations (Ref. [18]).

Clear critical point structures in Cu_2ZnSnS_4 ε can be seen in Fig. 4, that correspond to Van Hove singularities in the joint density of states [8]. The notations of the major critical points of Cu_2ZnSnS_4 in Fig. 4 were adopted from those of $CuInSe_2$ [17], based on the similarity between their lattice structures [18]. To deduce the CP energies, the ε spectra were smoothed with fast Fourier transform filtering, and then the second derivative $d^2\varepsilon/dE^2$ were taken and fit to an expression based on the parabolic band approximation and Lorentzian broadening:

$$\varepsilon = \sum_n \{A_n[\exp(i\phi_n)][E_n - E - i(\Gamma_n/2)]^{\mu_n}\} \qquad (1)$$

where A_n, E_n, Γ_n, μ_n, and ϕ_n are the amplitude, transition energy, broadening parameter, exponent, and phase, respectively, of the n^{th} critical point [8]. The exponent μ_n can take the value of ½, 0 ($\{[E_n\text{-}E\text{-}i(\Gamma_n/2)]^{\mu n}$ becomes $\ln[E_n\text{-}E\text{-}i(\Gamma_n/2)]\}$, -½, and −1, corresponding to 3D,

#160784 - $15.00 USD Received 19 Jan 2012; revised 13 Feb 2012; accepted 17 Feb 2012; published 7 Mar 2012

2D, 1D critical points, and discrete excitons [8]. Figure 5 shows the fits to the $d^2\varepsilon/dE^2$ spectra in the vicinity of selected CPs. The deduced transition energies and CP types are 1.32 (fundamental band gap, 2D), 2.92 (3D), 3.92 (3D), 4.96 (exciton), and 5.62 eV (exciton), for the E_0, E_1(A), E_1(B), E_2(A), and E_2(B) critical point, respectively.

Zhao and Persson calculated the theoretical optical properties of Cu_2ZnSnS_4, reproduced in Fig. 4, with a Green's function approach (GW method) [18]. Compared to the theoretical calculations, the experimental ε spectra have a lower amplitude and broader critical points, expectedly due to the scattering defects and possibly incorporated voids in the thin film [8]. The theoretical ε spectra have three distinct CP features (small circles) and one CP doublet (large circles), in possible correspondence to the CP structures observed in the experimental ε spectra except that they are blue shifted by ~0.3 to 1.0 eV, suggesting fine adjustments to the parameters used for the theoretical calculations. Nevertheless, considering the fundamental differences in these two studies, the agreement in Fig. 4 is reasonable.

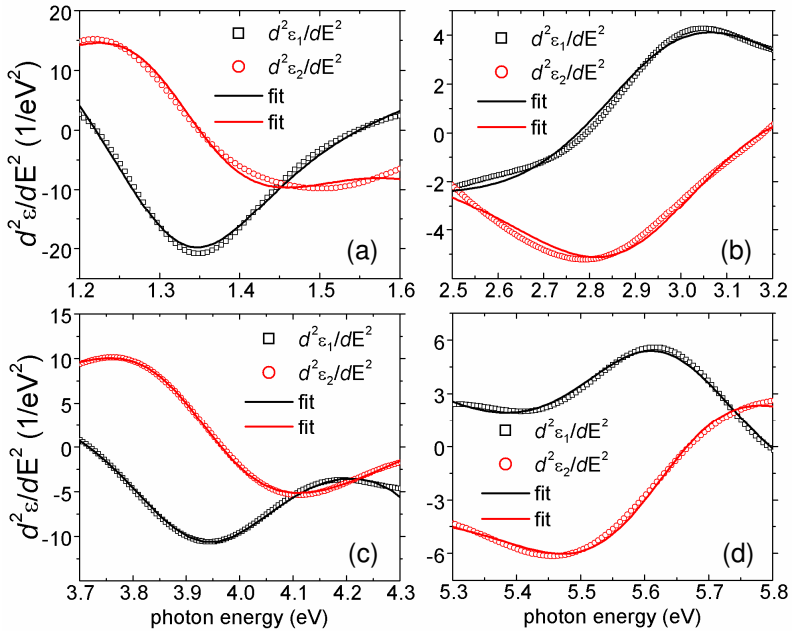

Fig. 5. The second derivative spectra of the experimental ε spectra in Fig. 4, and the model fits based on Eq. (1) used to deduce the transition energy of the (a) E_0, (b) E_1(A), (c) E_1(B), and (d) E_2(B) critical point.

Acknowledgments

This work was supported by the U.S. Department of Energy under Contract No. DE-AC36-08-GO28308 with NREL and by the University of Michigan under Subcontract No. XEJ-9-99035-01. The authors are grateful to H. Zhao and C. Persson of the Royal Institute of Technology (Sweden) for providing the numerical calculation results.